Low *Vp* and *Vp/Vs* zone beneath the northern Fossa Magna basin, central Japan, derived from a dense array observation

Eiji Kurashimo and Naoshi Hirata

The Earthquake Research Institute, the University of Tokyo, 1-1-1 Yayoi, Bunkyo-ku, Tokyo 113-0032, Japan

The northern Fossa Magna (NFM) basin is a Miocene rift system formed in the final stage of the opening of the Japan Sea. The northern part of the Itoigawa-Shizuoka Tectonic Line (ISTL) bounds the western part of the northern Fossa Magna. In order to understand the active tectonics in these areas, it is essential to explain the seismic velocity structures, deep structures of active faults, and microseismicity near the active faults. In the autumn of 2002, we conducted a seismic array observation across the northern part of the ISTL and the NFM to obtain a structural image beneath the NFM. Arrival times of local earthquakes and explosive shots were used in a joint inversion for earthquake locations and 3-D Vp and Vp/Vs structures. P- and S-wave arrival time data were obtained from 73 events including 4 explosive shots, and 3809 P- and 2659 S-wave arrival times were used for the inversion analysis. We obtained a seismic velocity model revealing good correlations with the surface geology along the profile. In particular, we found thick low-velocity zones beneath the NFM and the Komoro basin and a high-velocity zone beneath the Central Uplift Zone. Beneath the NFM, a low-velocity zone with low-to-moderate Vp/Vs extends to a depth of approximately 10 km. The low-velocity suggests the existence of aqueous fluid-filled pores with high aspect ratios.

Key words: Aqueous fluids, seismic velocity structure, travel time inversion, Itoigawa-Shizuoka Tectonic Line, Fossa Magna basin, Japan.

1. Introduction

The northern Fossa Magna (NFM) basin was formed as a back-arc rift during the final stage (ca. 17 Ma) of the opening of the Japan Sea (Sato *et al.*, 2004). The western part of the NFM is bounded by the Itoigawa-Shizuoka Tectonic Line (ISTL), which is one of the major tectonic boundaries in Japan (Fig. 1). The central-to-northern part of the ISTL is characterized as an active fault system, which shows one of the largest slip rates (4–9 mm/yr) in all of the Japanese islands (e.g., Miyauchi *et al.*, 2002). Across the northern part of the ISTL, recent GPS measurements indicate horizontal crustal shortening of approximately 0.3 ppm/yr (Sagiya *et al.*, 2002). A paleoseismological research reveals that the ISTL active fault system has a high potential for a large earthquake, indicating high seismic risk in surrounding areas (Okumura, 2001).

In order to understand the active tectonics in these areas, it is essential to explain the seismic velocity structures, deep structures of active faults, and microseismicity near the active faults. The Japanese islands, including the northern part of the ISTL, are covered with dense arrays of permanent seismic stations, which provide good constraints on velocity structures by a tomographic method. Such studies reveal a general picture of the lithospheric structure such as a descending plate configuration in the Chubu region, the central part of the Japanese islands (e.g., Sekiguchi, 2001).

However, since an average spacing of the permanent station is typically 20 to 30 km, a detailed structure in the upper crust, which is imperative for an understanding of the active tectonics, cannot be well constrained by permanent array alone. In the northern part of the ISTL, several controlled-source seismic experiments, including refraction and reflection profilings, were conducted (e.g., Asano *et al.*, 1969; Ikami *et al.*, 1986; Sakai *et al.*, 1996; Imai *et al.*, 2004). Although these studies shed light upon a shallow crustal heterogeneity in *P*-wave velocity (Vp) across the ISTL, limited data is available on the deeper crustal structure beneath the ISTL, particularly with respect to *S*-wave velocities (Vs). Since the Vp/Vs ratio is directly related to Poisson's ratio, it is a key parameter in the estimation of petrologic properties. In the autumn of 2002, we conducted a dense 60-km-long seismic array observation across the northern part of the ISTL active fault system and the NFM to obtain Vp and Vp/Vs structures. In this paper, we present a structural image beneath the northern Fossa Magna basin derived from a dense array observation.

2. Seismic Array Observation

We conducted a temporary seismic array observation across the northern part of the ISTL active fault system and the NFM (Fig. 2). Sixty 3-component portable seismographs were deployed along a 60-km-long linear array during the period from September 18, 2002 to November 2, 2002. Each seismograph consisted of a 1-Hz 3-component seismometer and a long-term low-power digital audio tape (DAT) recorder (Shinohara *et al.*, 1997). Waveforms were
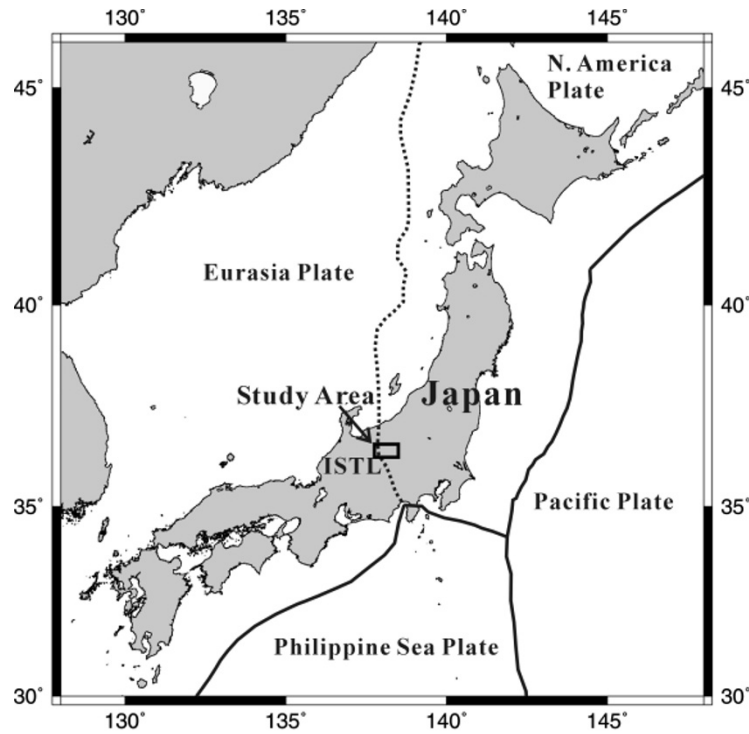
Fig. 1. Location map of the Itoigawa-Shizuoka Tectonic Line (ISTL), which is one of the major tectonic boundaries in Japan. The broken line indicates a plate boundary between the Eurasian plate and the North American plate (Kobayashi, 1983; Nakamura, 1983). The framed area represents a study area.
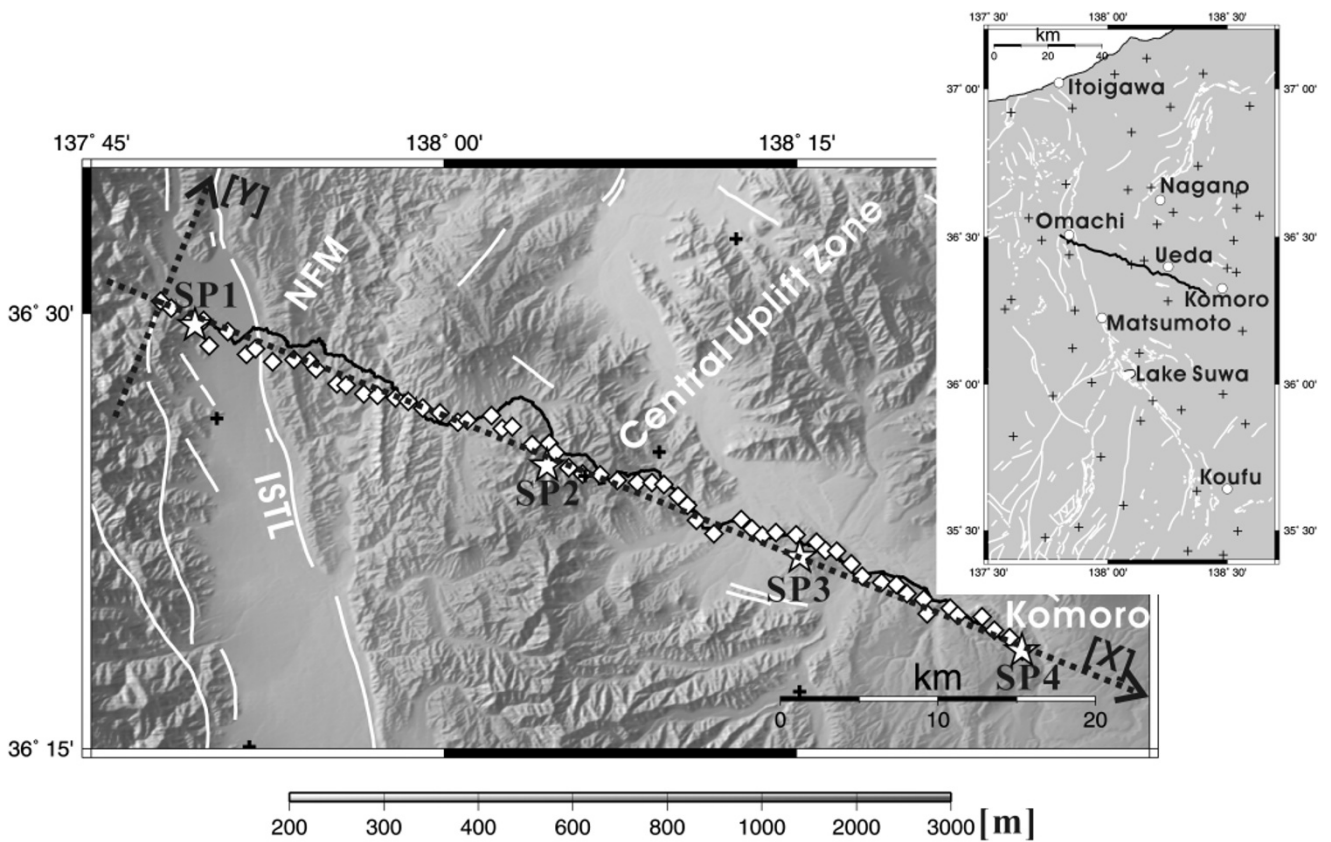

Fig. 2. Map showing the location of a seismic array observation across the northern part of the Itoigawa-Shizuoka Tectonic Line (ISTL) and the northern Fossa Magna (NFM) basin. The white lines indicate faults. Diamond and star symbols indicate temporary seismic stations and explosive shot points. The thick line indicates the deep seismic reflection and refraction/wide-angle reflection survey line (Sato *et al.*, 2004; Imai *et al.*, 2004). The X-Y coordinate system used in the 3-D inversion is also shown. The inset shows the distribution of the telemetered seismic stations used in the present study. The plus symbols indicate the telemetered seismic stations. The thick line indicates the location of the seismic array observation.
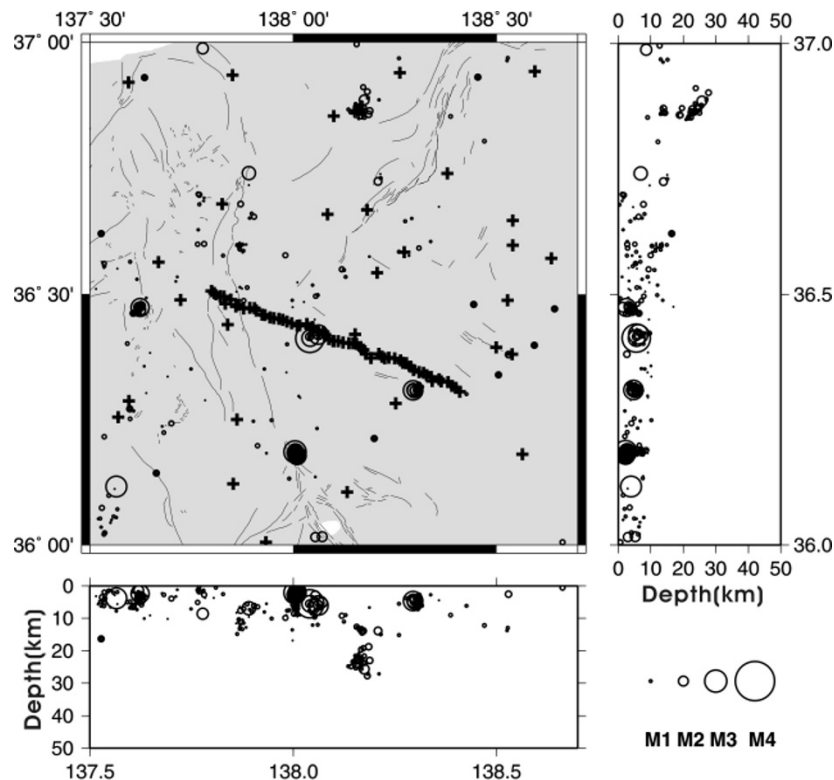
Fig. 3. Distribution of hypocenters determined by the JMA during the seismic array observation (from September 18, 2002 to November 2, 2002). During the seismic array observation, the JMA located 346 earthquakes in this area. The circle symbols are scaled to earthquake magnitude. The plus symbols indicate seismic stations used in the present study. The thin lines indicate faults.

continuously recorded at a sampling rate of 100 Hz. The DAT recorder included a Global Positioning System (GPS) receiver to maintain an accuracy of an internal clock of the recorder. Seismographs were installed with a spacing of approximately 1 km in order to obtain a crustal structure in detail. In the area of the present study, deep seismic reflection and refraction/wide-angle reflection profilings were conducted using vibrators and explosive sources (Sato *et al.*, 2004). The DAT recorders observed the controlled seismic signals as well as natural earthquakes.

3. Data

The continuously recorded data obtained by the DAT recorders were processed in the laboratory subsequent to the observations. First, they were divided into event files, each of which had waveform data that started from an origin time determined by the Japan Meteorological Agency (JMA) or the shot time of an explosion. In order to obtain a high-resolution velocity model, a well-controlled hypocenter is essential. Due to this, we combined the seismic array data recorded by the DAT with telemetered seismic data obtained by the Earthquake Research Institute, the University of Tokyo, the National Research Institute for Earth Science and Disaster Prevention, and the JMA. We used 52 telemetered seismic stations in the present study (Fig. 2). During the seismic array observation, the JMA located 346 earthquakes in a latitude range of 36°–37°N and a longitude range of 137.5°–138.7°E (Fig. 3). We selected 69 local crustal events so that they were distributed uniformly in the study area. We picked *P*- and *S*-wave arrivals of 73 events,
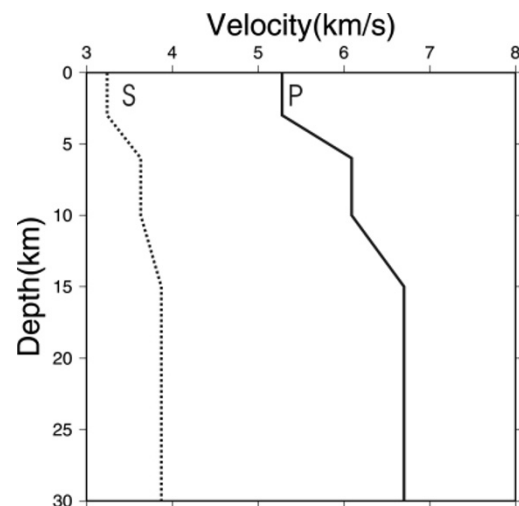

Fig. 4. Initial 1-D velocity model for 3-D inversion. The solid line denotes *P*-wave velocity, while the broken line denotes *S*-wave velocity. The values of Vp/Vs in the initial 1-D velocity model are 1.63 at depths of 0 to 3 km, 1.68 at 6 to 10 km, and 1.73 at a depth below 15 km.

including 69 local earthquakes and 4 explosive shots, at 112 stations. We obtained 3809 *P*- and 2659 *S*-wave arrival times, which were used in the inversion analysis. We estimated errors of 0.01–0.03 s in picking for *P*-arrival and those of 0.02–0.07 s for *S*-arrival.
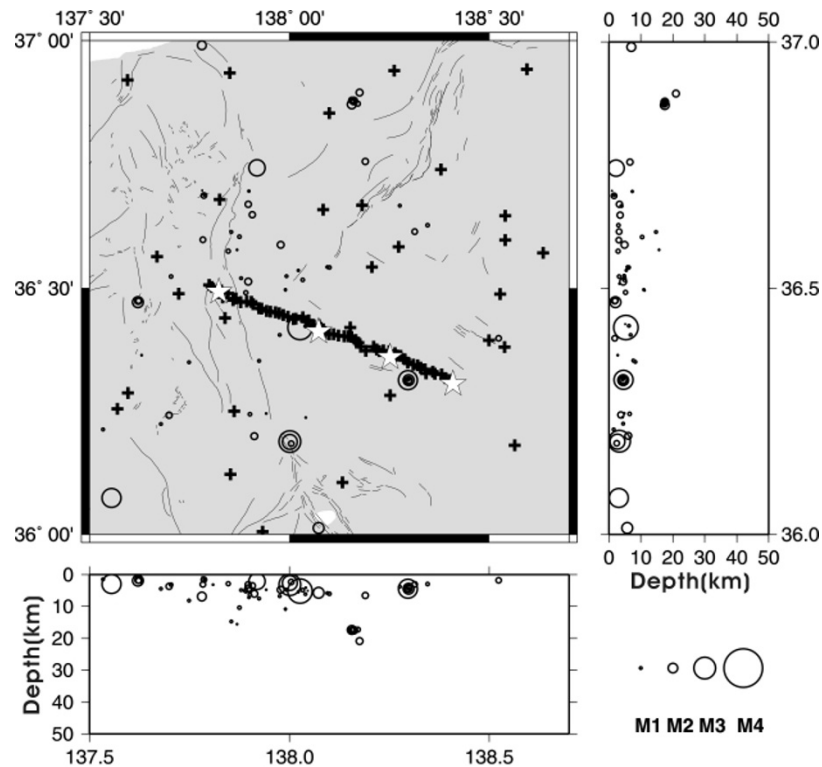
Fig. 5. Map showing the location of 69 final hypocenter distribution based on relocation in the 3-D velocity structure and 4 explosive shot points. P- and S-wave arrival times were obtained from 73 events (69 local earthquakes and 4 explosive shots) at 112 stations, which were used in the inversion analysis. The circle symbols are scaled to earthquake magnitude. Explosive shot positions are denoted by star symbols. The plus symbols indicate the seismic stations used in the present study. The thin lines indicate faults.

4.   Travel Time Inversion

The arrival times for the first P- and S waves obtained from 69 local earthquakes and 4 explosive shots were used in a joint inversion for earthquake locations and three-dimensional (3-D) Vp and Vp/Vs structures, using the iterative damped least-squares algorithm, *simul2000* (Thurber and Eberhart-Phillips, 1999). In *simul2000*, the Vp and Vp/Vs ratios are estimated at the nodes of a 3-D grid. We used an x-y co-ordinate system with the x-axis pointing N112°E and the y-axis pointing N22°E (Fig. 2). We used grid nodes with a spacing of 5 km in the X direction and a spacing of 20 km in the Y direction. In the vertical direction (Z), we tested several different spatial arrangements of grids between 3 and 5 km for the shallowest layers. Finally, we set the grid node at depths of −1, 0, 3, 6, 10, 15, 20, 25, and 30 km. Damping parameters are essential and critical during the inversion. Following Eberhart-Phillips (1986), we selected the appropriate damping by evaluating trade-off curves between the data and model variance. The solution of an inverse problem of 3-D local earthquake tomography and its reliability strongly depend on the initial one-dimensional (1-D) velocity model (e.g., Kissling, 1988). The initial 1-D velocity model used in the present study (Fig. 4) was obtained by resampling the 1-D velocity model calculated by the joint hypocenter determination (JHD) technique (Kissling *et al*., 1994) at the depths of the vertical grid nodes. The values of Vp/Vs in the initial 1-D velocity model are 1.63–1.73. The JHD technique simultaneously estimates the 1-D velocity model, earthquake locations, origin times, and stations corrections. These esti-

mates are used in this study as initials for the 3-D inversion. The final 3-D model achieved a 42% reduction in the root-mean-square (RMS) travel time residual in comparison with the initial 1-D velocity model. The distribution of hypocenters after the 3-D inversion is shown in Fig. 5.

5.   Solution Quality

A meaningful and reliable interpretation of the tomographic results requires an accurate analysis of the solution quality. We used diagonal elements of a resolution matrix to estimate the solution quality; these elements are shown in Figs. 6(b) and 6(d). The resolution is observed to be larger than 0.4 in the most part of the crust shallower than 10 km, a depth at which reliable results can be obtained (Thuber *et al*., 2003). We should notice that the easternmost part of the profile has a resolution less than 0.4, where the result is not considered to be reliable. We also carried out a checkerboard resolution test to confirm the adequacy of the evaluation of the resolution matrix. Synthetic reconstructions of the checkerboard velocity models were used to provide constraints on the resolution of the velocity model uncertainty. We assigned positive or negative velocity perturbations of ±10% in Vp and Vp/Vs to the grid nodes. The synthetic P- and S-wave arrival times for the checkerboard model were computed using the same source-receiver distribution of the real data. We then inverted them with an initial model of zero velocity perturbations, using the same parameterization as that for the real data. Results of checkerboard resolution tests (Vp and Vp/Vs) on a vertical cross-section along the x-axis ($Y = 0$ km) are shown in Fig. 7. The checker-
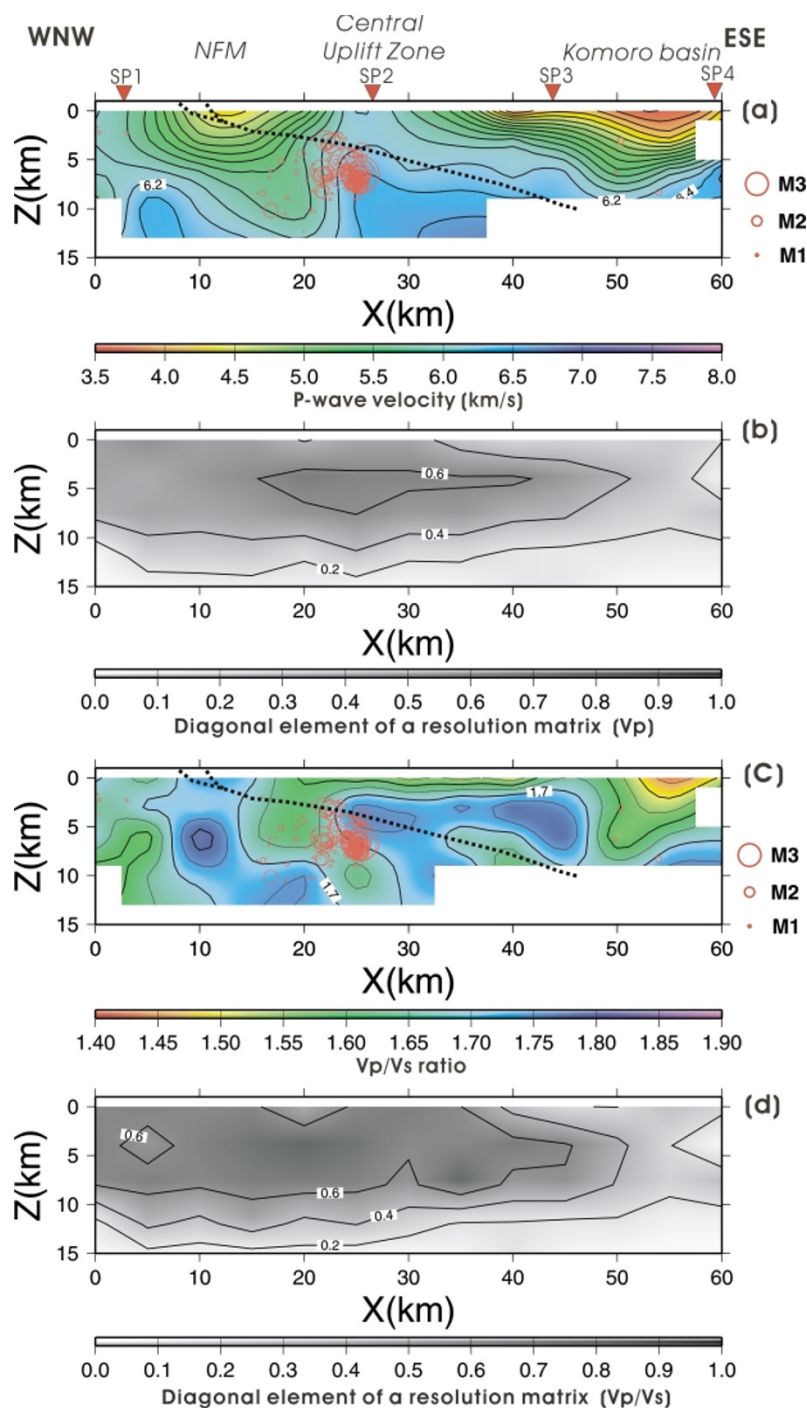
Fig. 6. Vertical cross-sections of the inverted P-wave velocity and Vp/Vs distribution along the x-axis ($Y = 0$ km). The explosive shot positions are denoted by red triangles at the top of figure. The thick broken line indicates the geometry of the ISTL active fault inferred from deep seismic reflection profiling (Sato *et al.*, 2004). The red circles denote hypocenters calculated by Sakai (2004) during the period from January 1, 2001 to January 21, 2004. Hypocenters within $Y = \pm 2$ km are shown. The circle symbols are scaled to earthquake magnitude. (a) P-wave velocity structure. Solid counter lines indicate Vp in km/s. The counter interval is 0.2 km/s. P-wave velocity is also indicated by color scale in km/s. Areas with resolution value less than 0.2 are painted white. (b) Diagonal elements of a resolution matrix (Vp). Solid counter lines indicate the resolution value. The counter interval is 0.2. The resolution value is also indicated by gray scale. (c) Vp/Vs distribution. Solid counter lines indicate the Vp/Vs ratio. The counter interval is 0.05. The Vp/Vs ratio is also indicated by color scale. Areas with resolution value less than 0.2 are painted white. (d) Diagonal elements of a resolution matrix (Vp/Vs). Same as Fig. 6(b), except for Vp/Vs.

board patterns are reproduced to a depth of approximately 10 km (Fig. 7), where the diagonal elements of a resolution matrix are larger than 0.2.

6. Results and Discussion

The vertical cross-sections of the inverted Vp and Vp/Vs distributions along the x-axis ($Y = 0$ km) are shown in Fig. 6. An example of the observed seismograms (vertical component) recorded by the DAT for natural earthquakes
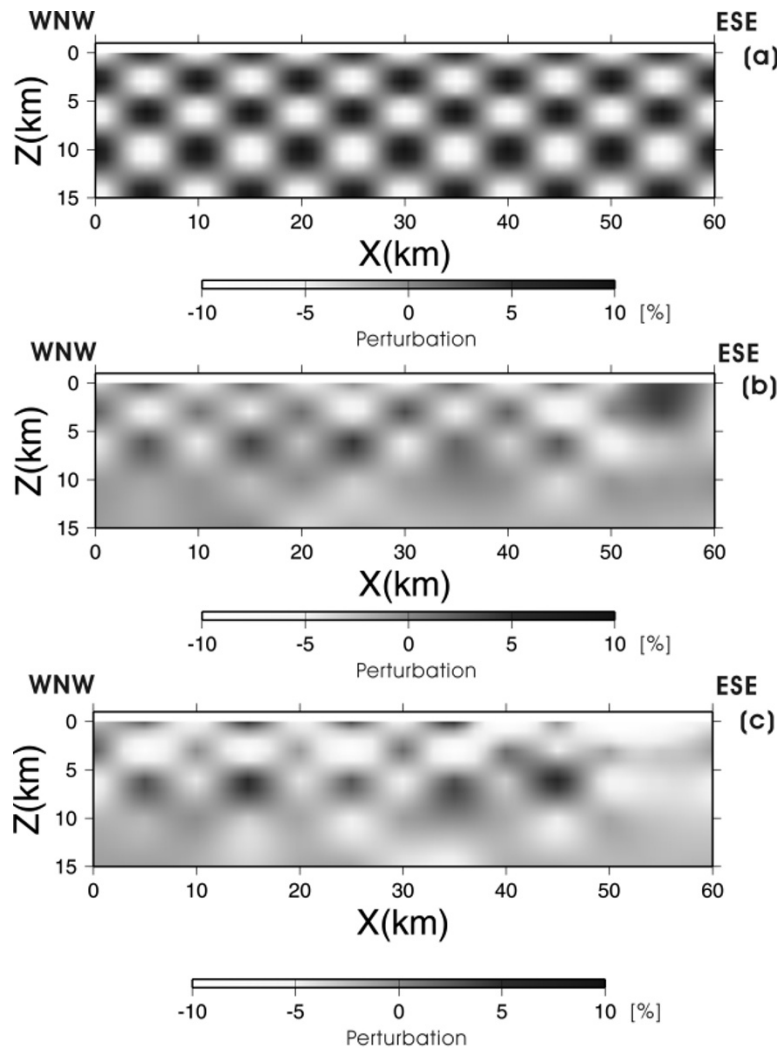
Fig. 7. Results of checkerboard resolution test on a vertical cross-section along the x-axis ($Y = 0$ km). The perturbations are indicated by gray scale in %. (a) Assigned perturbation of Vp and Vp/Vs: The maximum perturbation is 10%. (b) Results of checkerboard resolution test for Vp. (c) Results of checkerboard resolution test for Vp/Vs.

(36.604°N–137.875°E, 10.37 km deep, $M = 1.2$) is shown in Fig. 8. We also show calculated travel times with the seismograms and ray diagrams for the final model (Fig. 8). Calculated P- and S-wave arrival times explain the observed travel times well.

The prominent features in Fig. 6(a) are a high-velocity zone located in the horizontal range of 25–35 km and low-velocity zones located beneath both sides of the survey line. At a shallow depth, the Vp structure is consistent with the high-resolution refraction model of Imai *et al.* (2004). The present Vp model can be compared with the surface geology (Sato *et al.*, 2004), the resistivity model across the ISTL revealed by a magneto-telluric (MT) survey (Ogawa *et al.*, 2002), and the seismic tomography image beneath the Hida Mountains (Matsubara *et al.*, 2000), which overlaps with the western edge of the velocity model obtained in the present study. The velocity structure beneath the NFM, which consists of strongly folded Miocene marine sediments, is characterized by a low-velocity zone that thickens toward the east. Station corrections for P- and S-waves are also positive (0.2 s for P, 0.4 s for S), suggesting that low-velocity materials exist at very shallow depths. A high-velocity zone outcrops in the western end of the profile, which is also recognized at the eastern edge of the seismic tomography image of Matsubara *et al.* (2000), and it descends eastward. The high velocity zone may represent a Pre-Neogene basement. The Central Uplift Zone, which is composed of gently dipping lower Miocene submarine mudstone and volcanic rocks, is characterized by a slightly high-velocity zone situated at a shallow depth. The resistive zone beneath the Central Uplift Zone (Ogawa *et al.*, 2002) almost coincides with the high velocity zone. At the east of the Central Uplift Zone, the Komoro basin is characterized by a low-velocity zone.

Figure 6(c) shows a vertical cross-section of the inverted Vp/Vs distribution along the x-axis ($Y = 0$ km). Beneath the NFM, in the footwall of the ISTL active fault, a low Vp zone extends to a depth of approximately 10 km (Fig. 6(a)), where a low-to-moderate Vp/Vs (1.6–1.7) zone (Fig. 6(c)) exists. At a depth of 10 km, Vp is 5.6–5.8 km/s, approximately 8% lower than the average velocity at an equivalent depth. The low Vp at this depth generally suggests the existence of fluid in the crust or mantle, such as molten rock or aqueous fluid (e.g., Zhao *et al.*, 1996; Nakajima *et al.*,
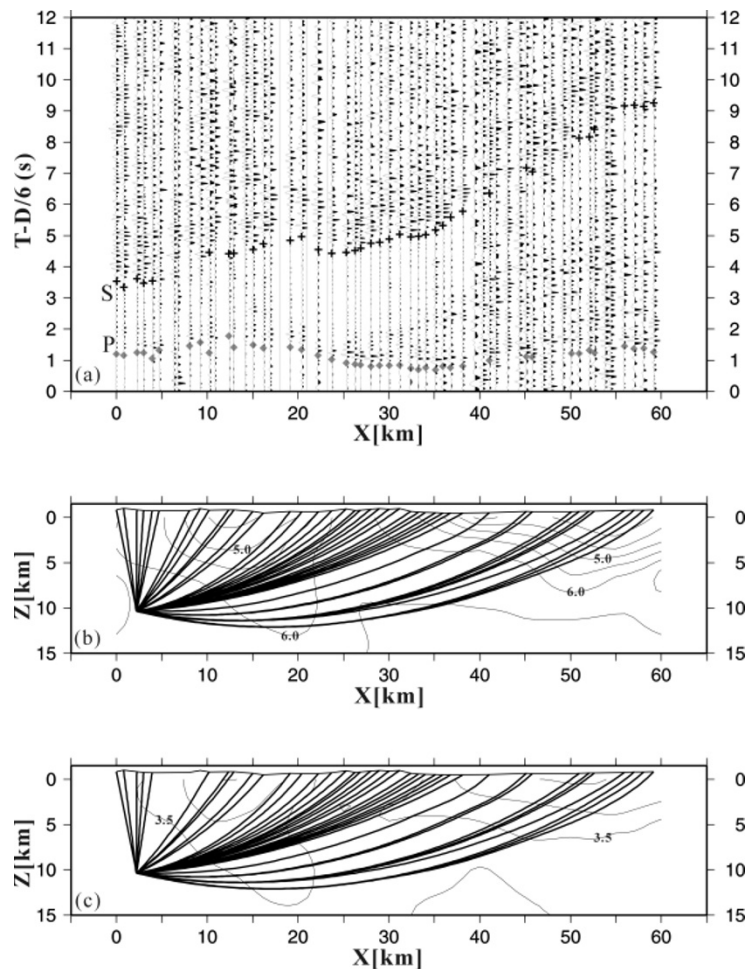
Fig. 8. Observed seismograms (vertical component) recorded by the DAT, calculated travel times, and ray diagrams for natural earthquake (36.604°N–137.875°E, 10.37 km deep, $M = 1.2$). Horizontal axis represents the x-axis ($Y = 0$ km). (a) Observed seismograms of the vertical component. Band-pass filter (1–10 Hz) and automatic gain control with 3-s window are applied. D: epicentral distance. The reduction velocity is 6 km/s. Calculated P-wave arrival times (diamond symbols) and S-wave arrival times (cross symbols) for the final model are superimposed on the observed seismograms. (b) Ray diagram of P-wave for the final model. Solid counter lines indicate Vp in km/s. The counter interval is 0.5 km/s. (c) Ray diagram of S-wave for the final model. Solid counter lines indicate Vs in km/s. The counter interval is 0.5 km/s.

2001; Zhao *et al.*, 2002; Nakajima and Hasegawa, 2003; Matsubara *et al.*, 2004). Nakajima *et al.* (2001) concluded that low velocity with low Vp/Vs zones in the upper crust are caused by the inclusion of H_2O and that low velocity with high Vp/Vs zones in the lower crust and the uppermost mantle are caused by melt inclusions. An MT survey conducted beneath the Hida Mountains revealed a highly conductive zone located at a depth of below 15–20 km (Ogawa *et al.*, 2002); this is consistent with the low velocity with high Vp/Vs (2.7) zone (Matsubara *et al.*, 2000). Matsubara *et al.* (2000) inferred that the low velocity anomaly can be explained by the partially melting rock. Although the studied area is in close proximity to the volcanic areas in the Hida Mountains, the existence of the low-velocity zone with low-to-moderate Vp/Vs has been noted. The relatively low Vp/Vs can be explained by the presence of an aqueous fluid in the pores: H_2O-filled pores with high aspect ratios. According to Takei (2002), the estimation of an aspect ratio of a H_2O-filled pore and a volume fraction of H_2O is possible using the ratio of fractional changes in Vp and Vs. The fractional change in Vp or Vs was evaluated on the basis of their velocity perturbations to the average

velocity of $Vp = 6.2$ km/s at an equivalent depth of 10 km. We obtained an aspect ratio of 0.02–0.1 and a volume fraction of 1–3% for the low-to-moderate Vp/Vs 1.6–1.7. The MT survey conducted beneath the NFM revealed a highly conductive zone located at a depth below 10 km (Ogawa *et al.*, 2002). They attributed the existence of a high conductive zone to the presence of fluids. The velocity structure image obtained in the present study suggests the existence of aqueous fluid-filled pores, which is consistent with the MT structure. Imai *et al.* (2004) report a seismic reflective zone located beneath the NFM at a depth below 11 km, which also suggests the existence of fluids in the mid-to-lower crust.

Sakai (2004) relocated micro-earthquakes in and around the northern part of the ISTL in consideration of the velocity structures obtained by refraction/wide-angle reflection profilings, as shown by open circles in Figs. 6(a) and 6(c). Few events are located within the low Vp and low-to-moderate Vp/Vs zone beneath the NFM. Most earthquakes in this area are concentrated in a depth range of 3–10 km (Sakai, 2004). In the 1960s, numerous small earthquakes occurred around Matsushiro, which is 30 km northeast of the stud-

ied area. The Matsushiro earthquake swarm was estimated to be caused by the eruption of water from the deep crust or mantle (e.g., Nakamura, 1971). These studies suggest that the presence of rheological change caused by localized aqueous fluid beneath the NFM may contribute to high seismicity in a narrow region.

7. Conclusion

We conducted a seismic array observation across the northern part of the ISTL active fault system and the NFM in order to obtain a structural image. P- and S-wave arrival time data were obtained from 73 events and 3809 P- and 2659 S-wave arrival times were used for the inversion analysis. The P-wave velocity structure along the profile shows that low-velocity zones exist beneath the NFM and the Komoro basin. The Central Uplift Zone is characterized by a relatively high-velocity zone. Beneath the NFM, a low-velocity zone with low-to-moderate Vp/Vs extends to a depth of approximately 10 km. Few earthquakes occur within this zone. The low velocity suggests the existence of aqueous fluid-filled pores with high aspect ratios. Beneath the NFM, a highly conductive zone is located at a depth below 10 km depth (Ogawa *et al.*, 2002). Most earthquakes in this area are concentrated in a depth range of 3–10 km above the reflective zone (Imai *et al.*, 2004; Sakai, 2004). These studies suggest that the presence of rheological change caused by localized aqueous fluid beneath the NFM may contribute to high seismicity in a narrow region.

References

Asano, S., K. Ichikawa, H. Okada, S. Kubota, H. Suzuki, M. Nogoshi, H. Watanabe, K. Seya, K. Noritomi, and K. Tazime, Explosion seismic observation in the Matsushiro earthquake swarm area, Spec. Rep. Geol. Survey of Japan, 5, 1969.

Eberhart-Phillips, D., Three-dimensional velocity structure in the northern California Coast Ranges from inversion of local earthquakes arrival times, *Bull. Seismol. Soc. Am.*, **76**, 1025–1052, 1986.

Ikami, A., T. Yoshii, S. Kubota, Y. Sasaki, A. Hasemi, T. Moriya, H. Miyamachi, R. S. Matsu'ura, and K. Wada, A seismic-refraction profile in and around Nagano prefecture, central Japan, *J. Phys. Earth*, **34**, 467–474, 1986.

Imai, T., T. Iwasaki, T. Takeda, T. Kawanaka, and H. Sato, Detailed upper crustal structure across the Itoigawa-Shizuoka Tectonic Line from the 2002 seismic expedition, Abstr, Japan Earth and Planetary Science 2004 Joint Meeting, S075–005, 2004.

Kissling, E., Geotomography with local earthquake data, *J. Geophys. Res.*, **93**, 1073–1085, 1988.

Kissling, E., W. L. Ellsworth, D. Eberhart-Phillips, and U. Kradolfer, Initial reference models in local earthquake tomography, *J. Geophys. Res.*, **99**, 19635–19646, 1994.

Kobayashi, Y., Initiation of plate subduction, *Earth Monthly*, **3**, 510–518, 1983 (in Japanese).

Matsubara, M., N. Hirata, S. Sakai, and I. Kawasaki, A low velocity zone beneath the Hida Mountains derived from dense array observation and tomographic method, *Earth Planets Space*, **52**, 143–154, 2000.

Matsubara, M., N. Hirata, H. Sato, and S. Sakai, Lower crustal fluid distribution in the northeastern Japan arc revealed by high-resolution 3D seismic tomography, *Tectonophysics*, **388**, 33–45, 2004.

Miyauchi, T., Y. Ikeda, T. Imaizumi, M. Togo, H. Sato, and N. Matsuta, Active fault system in the northern Fossa Magna basin, in *Atlas of Quaternary Thrust Faults in Japan,* edited by Y. Ikeda *et al.*, pp. 148–161, Univ. of Tokyo Press, Tokyo, 2002 (in Japanese).

Nakajima, J. and A. Hasegawa, Tomographic imaging of seismic velocity structure in and around the Onikobe volcanic area, northeastern Japan: Implication for fluid distribution, *J. Volcanology Geothermal Res.*, **127**, 1–18, 2003.

Nakajima, J., T. Matsuzawa, A. Hasegawa, and D. Zhao, Three-dimensional structure of Vp, Vs, and Vp/Vs beneath northeastern Japan: Implications for arc magmatism and fluids, *J. Geophys. Res.*, **106**, 21843–21857, 2001.

Nakamura, K., A hypothesis on mechanism of the Matsushiro earthquake swarm, *Kagaku-Asahi*, **10**, 127–133, 1971 (in Japanese).

Nakamura, K., Possible nascent trench along the eastern Japan Sea as the convergent boundary between Eurasian and North American plates, *Bull. Earthq. Res. Inst. Univ. Tokyo*, **58**, 711–722, 1983 (in Japanese).

Okumura, K., Paleoseismology of the Itoigawa-Shizuoka Tectonic Line in central Japan, *Jour. Seismol.*, **5**, 411–431, 2001.

Ogawa Y., S. Takakura, and Y. Honkura, Resistivity structure across Itoigawa-Shizuoka Tectonic Line and its implications for concentrated deformation, *Earth Planets Space*, **54**, 1115–1120, 2002.

Sagiya, T., T. Nishimura, Y. Iio, and T. Tada, Crustal deformation around the northern and central Itoigawa-Shizuoka Tectonic Line, *Earth Planets Space,* **54**, 1059–1063, 2002.

Sakai, S., Seismicity of the northern part of Itoigawa-Shizuoka Tectonic Line, Abstr, Japan Earth and Planetary Science 2004 Joint Meeting, S075-P005, 2004.

Sakai, S., T. Iwasaki, T. Iidaka, T. Yoshii, F. Yamazaki, and T. Kuwayama, The structure of the crust of Chubu region from the extension observation, *Earth Monthly,* **18**, 104–108, 1996 (in Japanese).

Sato, H., T. Iwasaki, S. Kawasaki, Y. Ikeda, N. Matsuta, T. Takeda, N. Hirata, and T. Kawanaka, Formation and shortening deformation of back arc rift basins revealed by deep seismic profiling across the Itoigwa-Shizuoka Tectonic Line active fault system, *Tectonophysics*, **388**, 47–58, 2004.

Sekiguchi, S., A new configuration and an aseismic slab of the descending Philippine Sea plate revealed by seismic tomography, *Tectonophysics*, **341**, 19–32, 2001.

Shinohara, M., N. Hirata, and S. Matsuda, Long-term low-power DAT seismic digital data recorder with GPS clock, *Zisin*, **50**, 119–124, 1997 (in Japanese with English abstract).

Takei, Y., Effect of pore geometry on Vp/Vs: From equilibrium geometry to crack, *J. Geophys. Res.*, **107**(B2), 2043, 10.129/2001JB000522, 2002.

Thurber, C. and D. Eberhart-Phillips, Local earthquake tomography with flexible gridding, *Comp. Geosci.*, **25**, 809–818, 1999.

Thurber, C., S. Roecker, K. Roberts, M. Gold, L. Powell, and K. Rittger, Earthquake locations and three-dimensional fault zone structure along the creeping section of the San Andreas fault near Parkfield, CA: Preparing for SAFOD, *Geophys. Res. Lett.*, **30**(3), 1112, doi:10.1029/2002GL016004, 2003.

Zhao, D., H. Kanamori, H. Negishi, and D. Wiens, Tomography of the source area of the 1995 Kobe earthquake: Evidence for fluids at the hypocenter?, *Science*, **274**, 1891–1894, 1996.

Zhao, D., O. P. Mishra, and R. Sanda, Influence of fluids and magma on earthquakes: Seismological evidence, *Phys. Earth Planet. Inter,* **132**, 249–267, 2002.

E. Kurashimo (e-mail: ekura@eri.u-tokyo.ac.jp) and N. Hirata